2023 IEEE International Conference on Robotics and Automation (ICRA 2023)
May 29 - June 2, 2023. London, UK

Image-Based Visual Servoing Switchable Leader-follower Control of Heterogeneous Multi-agent Underwater Robot System

Kanzhong Yao[1], Nathalie Bauschmann[2], Thies L Alff[2], Wei Cheah[1], Daniel A Duecker[2,3], Keir Groves[1], Ognjen Marjanovic[1], and Simon Watson[1]

***Abstract*— Confined and cluttered aquatic environments present a number of significant challenges with respect to inspection by robotic platforms, including localisation and communications. Some of these can be mitigated by using collaborative heterogeneous multi-robot teams. An important element of such a system is collaborative control. This paper addresses this challenge by presenting an Image-Based Visual Servoing (IBVS), leader-follower control system for heterogeneous aquatic robots. Experiments were conducted in an uncluttered pond to demonstrate the capabilities of the system. The results show robots can maintain tracking each other with maximum x and y displacements of 0.42 m and 0.41 m, the maximum projection distance in the xy-plane of maintaining formation is 0.45 m, showing the stability and feasibility of deploying such system on underwater platforms.**

I. INTRODUCTION

Aquatic robot inspection systems can be used to access challenging and complex environments which humans cannot access or which pose significant safety issues [1]. These environments often bring constraints in localisation and communication to the robot systems, especially in those scenarios that involve confined spaces such as nuclear fuel pond inspection, underwater pipeline maintenance, or unknown aquatic environment exploration.

These missions require the robot to maximize the maneuvering envelope whilst localising itself in a cluttered environment with no external infrastructure [2]. Systems consisting of more than one robot have been shown to execute objectives more efficiently and reliably under such constraints [3].

A. Background and Mission Definition

A range of confined and challenging environments that require robotic inspection are presented in [1]. These environments are accessible to both the surface and sub-surface vehicles and are, therefore, well suited to the exploration conducted by multi-robot teams. An autonomous surface vehicle (ASV) was presented in [4], which is able to localise itself with mm range accuracy within a confined environment using a 2D LiDAR.

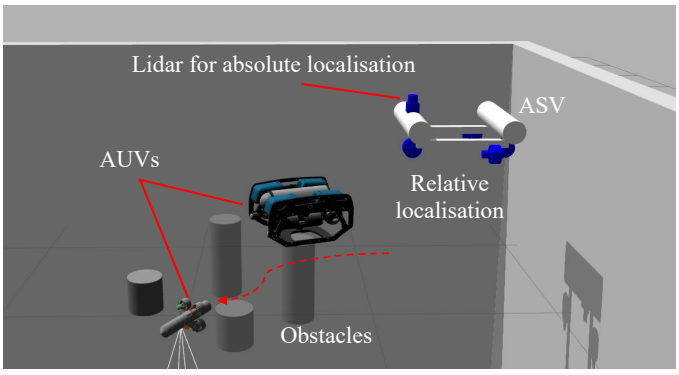

Fig. 1. Mission scenario: Heterogeneous multi-agent underwater system with ASV/AUVs working cooperatively to localise each other and explore obscured confined aquatic areas.

If this ASV is coupled to an autonomous underwater vehicle (AUV) by using a vision-based relative localisation system, the absolute position of the AUV could be estimated (albeit with a higher error). As long as there is direct line-of-sight (LoS) and clear visibility, this would allow sensor data gathered by the AUV to be geolocated within the environment without the need for external infrastructure or environmental features (as required by vision-based SLAM systems). This approach could also be 'daisy-chained' where multiple AUVs localise each other (with decreasing localisation accuracy), which could enable exploration of obscured areas, as shown in Fig.1.

To enable autonomous operation using this approach requires three elements; an ASV with absolute localisation capabilities [4]; a vision-based relative localisation system [5] and a collaborative leader-follower control algorithm, which is the subject of this paper. When executing missions in unknown underwater environments, full exploration coverage of the 3D space can be described as a series of planar scans performed at different depths. Such a control scheme [6] that covers 3D space in 2D slices is termed 2.5D control. This study will focus on such 2.5D control scheme which provides a basis for extending it to full 3D exploration in future development.

B. Related Work

Formation control is one of the key elements needed to achieve high-level autonomy in multi-agent robot systems

*This work was supported in part by Chinese Scholarship Council-University of Manchester joint programme, in part by the UK Turing Scheme and UKRI Grant EP/P01366X/1, and by an EPSRC Impact Acceleration Account Secondment Scheme, "Heterogeneous multi-agent robotic inspection missions" which was jointly funded by Sellafield Ltd, The University of Manchester and EPSRC.

[1] Manchester Centre for Robotics and AI, Department of Electrical and Electronic Engineering, University of Manchester, UK. Please direct correspondence to kanzhong.yao@postgrad.manchester.ac.uk

[2] Institute of Mechanics and Ocean Engineering, Hamburg University of Technology, Germany.

[3] Munich Institute of Robotics and Machine Intelligence (MIRMI), Technical University of Munich (TUM), Germany.

[7]. Among many formation control approaches such as sonar/laser-based unit-centre formation and neighbor coordination, vision-based leader-follower control is adopted in this paper due to its application scalability. Vision-based leader-follower control methods can be categorised into two types [8]: Position-Based Visual Servoing (PBVS) and Image-Based Visual Servoing (IBVS). PBVS tracks its target by calculating the relative pose based on camera parameters [9], while IBVS achieves formation by directly controlling the target position within the camera view [10]. Therefore, IBVS is more suitable for underwater environments as it is less dependent on camera calibration [11]. Besides, to maintain the Line-of-Sight (LoS) during formation movements while either of the robots may need to prioritise object avoidance in cluttered environments, both robots should have the capability of acting in the role of leader or follower in the leader-follower formation scheme.

In the past decade, progress has been made in leader-follower formation control. Consolini [12] proposed a formation control strategy in which a follower's position is not rigidly fixed with respect to the leader. This work contributes to the domain of leader-follower control with constrained input, which becomes an important basis of much of the subsequent related work [13]–[15]. For example, adaptive vision-based leader-follower control approaches have been proposed in [16] and [8] that rely on onboard visual sensors alone and require neither communication between two agents, nor the relative position measurement. However, these systems were limited to the application domain of ground-based/aerial robots. When applying these approaches to aquatic systems, there are several additional challenges with localisation, communication, unmodelled dynamics and camera distortions caused by the water.

With respect to underwater multi-agent robotic systems, [17] describes a systemic structure of cooperative control algorithms for underwater robots, which achieves cooperative navigation based on data transfer between robots. Based on relative position calculation, Bechlioulis [3] proposed a control architecture that addresses distance-based formation control for multi-AUV systems. In the WiMUST [18] project, coordinated trajectory tracking was achieved within a cooperative marine robotic system via acoustic communication. In [18], a flexible leader-follower control algorithm based on velocity measurement was proposed. In this work, the leader's velocity can either be communicated between the robots through deliberate cooperation, or the follower can estimate it using a perception approach. Existing multi-agent AUV systems, which achieve formation control, rely either on communication or on localisation (communication based velocity measurement), which are not applicable to our target scenarios.

C. Contribution

The contribution of this work is as follows:

- A switchable IBVS leader-follower control algorithm for multi-AUV systems is proposed and implemented on small aquatic robots.
- Physical demonstration and characterisation of leader-follower formation for heterogeneous AUVs with a 2.5D maneuvering scheme.

To the best of the author's knowledge, this is the first reported investigation and demonstration of IBVS leader-follower control algorithm on physical aquatic platforms.

The rest of this paper is organised as follows: Section II formulates the target problem to be addressed, Section III discusses the kinematic model and IBVS algorithm of our system, physical platform demonstration and experiments are carried out in Section IV as well as the discussion to the results, conclusions are drawn in Section V.

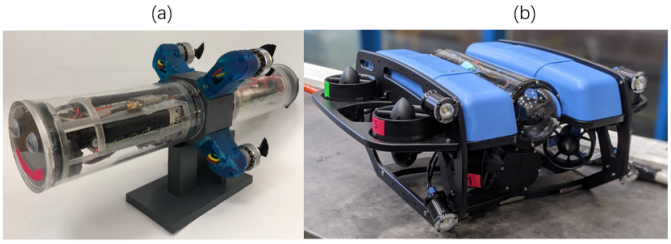

Fig. 2. Picture a) shows the HippoCampus micro Autonomous Underwater Vehicle (μAUV) [19], picture b) shows a commercial Remotely Operated Vehicles (ROV) BlueROV2 (heavy), which was also made autonomous.

II. PROBLEM FORMATION

The targeted research gap and potential solutions have been specified in former sections, the following discussion will be subject to constraints, goal and assumptions of this research.

- Constraints: unavailability of reliable and deployable underwater communication and localisation in confined spaces is impeding subsurface robotic missions.
- Goal: achieve leader-follower formation control without human intervention under communication and localisation denied condition, which makes autonomous underwater exploration possible.

Since on-board cameras are relatively easy to have on an AUV, we address this problem by introducing a switchable vision-based leader-follower control algorithm using the IBVS approach [11]. To design the control model of the system, two assumptions have to be made:

Assumption 1: at the starting point, leader is inside the follower's line-of-sight (LoS).

Assumption 2: leader's trajectory is within the follower's maneuver capability.

III. METHODOLOGY

In this section, we first derive the hydrodynamic model for both the leader and the follower under the same coordinate system. Next, we establish a leader-follower control scheme and the visual servoing model.

The two robots used in the composition of our heterogeneous system are HippoCampus (Fig.2.a) [19] and BlueROV2 (Fig.2.b). HippoCampus[1] is an open-source micro

[1]https://hippocampusrobotics.github.io/

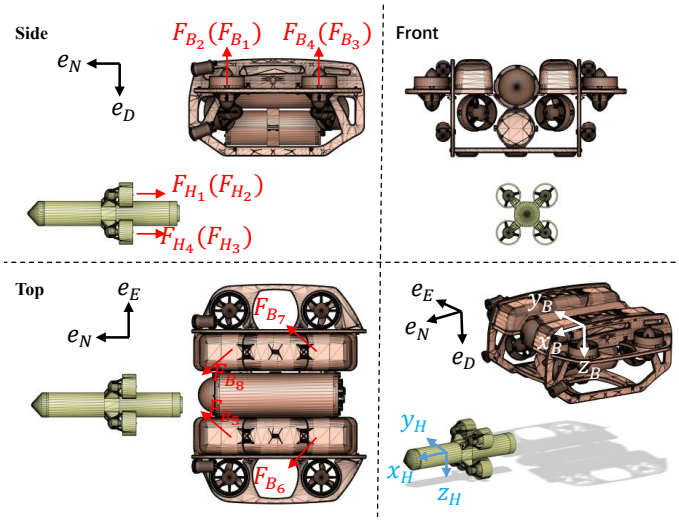

Fig. 3. Coordinate system and force distribution of HippoCampus (μAUV) and BlueROV2 (heavy). Black indicates the North-East-Down (NED) coordinates, blue and white show robot coordinates.

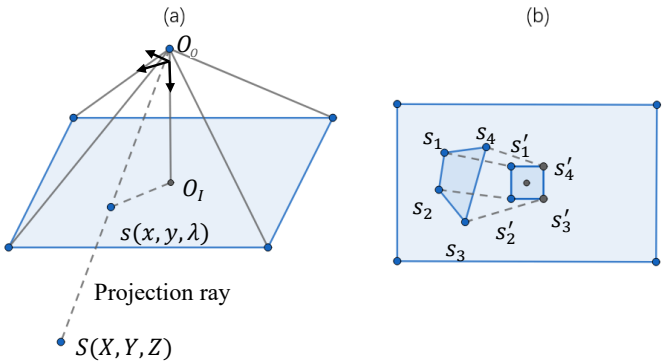

Fig. 4. Geometrical interpretation of Image Based Visual Servoing. (a) Pinhole camera model and projection of feature point S onto the image plane O_I. (b) Feature points of target image projected on the image plane.

underwater robotic platform with four propellers and the capability of agile maneuvering on complex trajectories. The BlueROV2 in its *heavy* configuration is a widely used fully actuated commercial underwater robotic research platform manufactured by BlueRobotics.

A. Dynamic Model

1) Notations: All frames in the following descriptions are in North-East-Down (NED) coordinates, where $\{e_N, e_E, e_D\}$ defines the inertial world frame $\{O_W\}$, $\{x_H, y_H, z_H\}$ and $\{x_B, y_B, z_B\}$ describe the base of body-fixed frames of HippoCampus $\{O_H\}$ and BlueROV2 $\{O_B\}$, as shown in Fig.3. For the following, the index f indicates expressions corresponding to either HippoCampus (H) or BlueROV2 (B), respectively.

2) Hydrodynamics: The mathematical model for both underwater vehicles used in this study is based on the concepts by Fossen [20]. The general dynamic equations for hydrodynamic motion can be written as

$$\begin{aligned} \dot{\boldsymbol{\eta}} &= \boldsymbol{J}(\boldsymbol{\eta})\,\boldsymbol{\nu}, \\ \boldsymbol{M}\dot{\boldsymbol{\nu}} + \boldsymbol{C}(\boldsymbol{\nu})\boldsymbol{\nu} + \boldsymbol{D}(\boldsymbol{\nu})\boldsymbol{\nu} + \boldsymbol{g}(\boldsymbol{\eta}) &= \boldsymbol{\tau}. \end{aligned} \tag{1}$$

Here, $\boldsymbol{J}(\boldsymbol{\eta})$ is the transformation matrix from body frame to world frame of f vehicle and $\boldsymbol{\eta} = [x, y, z, \phi, \theta, \psi]^\top$ represents the pose$\{O_f\}$ consisting of position and Euler angles. The vehicles' linear and angular velocities in the respective body-fixed frames are denoted by $\boldsymbol{\nu} = [u, v, w, p, q, r]^\top$. Furthermore, $\boldsymbol{M}$, $\boldsymbol{C}$, and $\boldsymbol{D}$ represent the individual inertia, damping, and Coriolis rigid body effects. This includes the fluid effects caused by added mass. Those values can be determined experimentally [21], [22]. Moreover, $\boldsymbol{g}(\boldsymbol{\eta})$ stands for the hydrostatic load composed by buoyancy and gravitational forces. $\boldsymbol{\tau}_f$ is the control input, representing the force vector generated by actuators. On the robot side, $\boldsymbol{\tau}_f$ can be decomposed into force F_i and moment M_i generated by the individual thruster i and then converted to the velocity of the robots in 6 Degree-of-Freedom (DoF) as

$$\boldsymbol{\tau}_f = \sum_{i=1}^{n} \begin{bmatrix} F_i \\ M_i + r_i \times F_i \end{bmatrix} = [u_x, u_y, u_z, u_\phi, u_\theta, u_\psi]^\top \tag{2}$$

for robot f, $\boldsymbol{r}_i$ is the vector from thruster i to the center of gravity, $u_{1:6}$ are the control inputs affecting the $[x, y, z, \phi, \theta, \psi]$ rates. The heavy configuration BlueROV2 is fully-actuated, where $F = F_{B,i}$, $i = \{1, ..., 8\}$, while the under-actuated HippoCampus $F = F_{H,i}$ where $i = \{1, ..., 4\}$. It is worth noting that for HippoCampus, $\boldsymbol{\tau}_H$ yields to $[u_x, 0, 0, u_\phi, u_\theta, u_\psi]^\top$.

B. Visual Servoing

1) Selection of method: As mentioned in Section I, with distortions generated underwater, IBVS was selected as our modeling basis to reduce the reliance on pose estimation and increase the robustness to inaccuracies in image measurements.

2) Modelling with selected approach: Generally, vision-based control schemes' aim is to minimise the error $\boldsymbol{e}(t)$, which can be defined by [11]

$$\boldsymbol{e}(t) = \boldsymbol{s}(\boldsymbol{m}(t), \delta) - \boldsymbol{s}_*. \tag{3}$$

where $\boldsymbol{m}(t)$ are the pixel coordinates of projected feature points of interest and δ describes the intrinsic camera parameters, which can be obtained from camera calibration. Moreover, $\boldsymbol{s}_*$ contains the desired values of the projected feature point. As shown in Fig.4(a), O_O is the origin of camera frame, s is the projection of feature point S onto the image plane O_I. The relationship between the camera's twist, $\boldsymbol{\nu}_O \in \mathbb{R}^6$ and the projection $\boldsymbol{s}$ is given by

$$\dot{\boldsymbol{s}} = \boldsymbol{L}_s\,\boldsymbol{\nu}_O \ , \tag{4}$$

where $\boldsymbol{L}_s \in \mathbb{R}^{k\times 6}$ is the interaction matrix [23] related to k feature points $\boldsymbol{s}$.

Let $S(X, Y, Z)$ and $s(x, y)$, $\boldsymbol{L_s}$ can be described by [11] reading

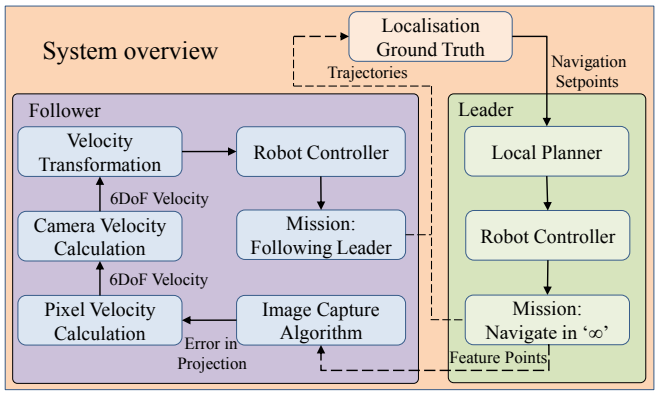

Fig. 5. Control loop of the system, including algorithms implemented on each robots for acting as leader and follower. Dash line indicates that there is no direct communication between two modules. Ground truth of trajectories is acquired for visualisation and analyses.

$$\boldsymbol{L_s} = \begin{bmatrix} -1/Z & 0 & x/Z & xy & -(1+x^2) & y \\ 0 & -1/Z & y/Z & 1+y^2 & -xy & -x \end{bmatrix} . \tag{5}$$

For the following, we select four feature points $(\boldsymbol{s}_1, \boldsymbol{s}_2, \boldsymbol{s}_3, \boldsymbol{s}_4)$. Furthermore, four corresponding target projection points $(\boldsymbol{s}'_1, \boldsymbol{s}'_2, \boldsymbol{s}'_3, \boldsymbol{s}'_4)$ are defined as shown in Fig.4(b). Thus, (4) becomes

$$\begin{bmatrix} \dot{\boldsymbol{s}}_1 \\ \dot{\boldsymbol{s}}_2 \\ \dot{\boldsymbol{s}}_3 \\ \dot{\boldsymbol{s}}_4 \end{bmatrix} = \begin{bmatrix} \boldsymbol{L}_{s_1} \\ \boldsymbol{L}_{s_2} \\ \boldsymbol{L}_{s_3} \\ \boldsymbol{L}_{s_4} \end{bmatrix} \boldsymbol{\nu}_O \ . \tag{6}$$

C. Leader-Follower Control Architecture

The BlueROV2 and HippoCampus body-rates and attitudes can be controlled directly. The camera velocity for target tracking from (6) can be transformed to the robot's velocity in (2) as follows

$$\begin{bmatrix} \dot{\boldsymbol{s}}_1 \\ \dot{\boldsymbol{s}}_2 \\ \dot{\boldsymbol{s}}_3 \\ \dot{\boldsymbol{s}}_4 \end{bmatrix} = \begin{bmatrix} \boldsymbol{L}_{s_1} \\ \boldsymbol{L}_{s_2} \\ \boldsymbol{L}_{s_3} \\ \boldsymbol{L}_{s_4} \end{bmatrix} \boldsymbol{T}_f \boldsymbol{K}_f [u_x, u_y, u_z, u_\phi, u_\theta, u_\psi]^\top , \tag{7}$$

where $\boldsymbol{T}_f$ represents the velocity transformation matrix from the body-fixed frame to the camera frame, $\boldsymbol{K}_f$ is diagonal tuning parameter matrix.

To achieve leader-follower formation control, the control scheme will be centered around the follower while the leader simply follows a specific trajectory. The systemic control loop that contains both the leader and follower robots is given in Fig. 5. No communication and localisation will be required between two vehicles to achieve the described leader-follower formation.

IV. Deployment and Analysis

Experimental deployment of the proposed system will be conducted and corresponding results will be analysed. A video of the experiments is available in the supplementary material.

A. Localisation and Navigation

In a real-world mission, absolute localisation could be achieved using underwater localisation system such as [2], [4], [24] to obtain ground truth of the robots. To evaluate the performance and reliability of the proposed leader-follower formation control scheme, the absolute localisation system developed in [5] was used to provide ground truth for the position of both robots, and to enable the leader AUV to autonomously follow a pre-defined trajectory with no human input. The controller for the leader is defined as

$$\begin{bmatrix} \boldsymbol{v} \\ \boldsymbol{\omega} \end{bmatrix} = \begin{bmatrix} \boldsymbol{K}_v \boldsymbol{e}_P \\ -\boldsymbol{K}_R \boldsymbol{e}_R - \boldsymbol{K}_\omega \boldsymbol{e}_\omega \end{bmatrix} \tag{8}$$

where $\boldsymbol{K}_v, \boldsymbol{K}_R$, and $\boldsymbol{K}_\omega$ are diagonal gain matrices, $\boldsymbol{e}_P$ is the position error, $\boldsymbol{e}_R$ describes the robot's orientation error with regard to the desired orientation, $\boldsymbol{e}_\omega$ is the error of the corresponding angular velocities. Since leader control is not the focus of this work, we refer to [25] for a detailed explanation of the underlying attitude control framework including the selection of parameters of $\boldsymbol{K}_v, \boldsymbol{K}_R$, and $\boldsymbol{K}_\omega$ in (8).

From (2) it can be seen that HippoCampus is a nonholonomic vehicle while BlueROV2 is holonomic. To overcome the reduction in manoeuvrability When HippoCampus is the follower, we set the leader's linear velocity constant as $[0.2, 0, 0]^\top$ which reduces the influence of the leader's controller on the overall cooperative control performance subject to assumption 2.

B. Hardware Setup

A single AprilTag is attached on the leader robot for providing feature points to calculate velocity in (7), specifically the four corners of the tag. The pose information of the tag is not used in any way. For future testing and real-world deployment, other sources of feature points provider such as salient LED of optical modem or active markers will be investigated to replace the Apriltag used in this study.

According to (2) and Fig 3, τ_B for BlueROV2 is $[u_x, u_y, u_z, u_\phi, u_\theta, u_\psi]^\top$ whilst τ_H for hippocampus yields to $[u_x, 0, 0, u_\phi, u_\theta, u_\psi]^\top$. Both BlueROV2 and Hippocampus have none zero u_ψ, which gives them the capability to rotate along its z axis and navigating within the test pond requires them to do so. Therefore, to meet the requirement of assumption two, leader robot should avoid generating none zero u_y for Hippocampus when rotating in z direction. Hence, tag providing feature points for tracking is placed centered with leader robot's z axis in our following tests (see Fig. 7).

The AprilTag family 36h11 with a side length of 9.6 cm is selected. On the sensing side, a Raspberry Pi camera with 640 × 480 px is selected for image capture. The VISP library [26] provides the foundation for the camera velocity calculation. ROS is used as the middleware for both hardware and software, as illustrated in Fig. 6. The robots used in the following tests are the BlueROV2 heavy configuration with an extra downward-facing camera and the HippoCampus μAUV. AprilTags pre-mounted on the tank

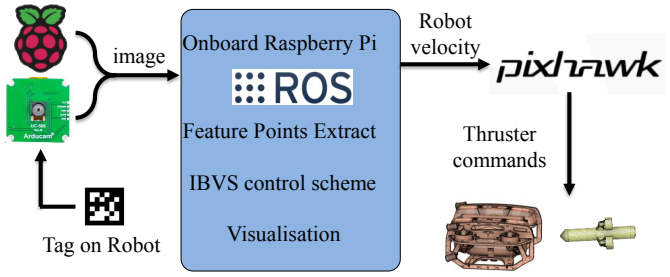

Fig. 6. Systemic hardware setup of the robot.

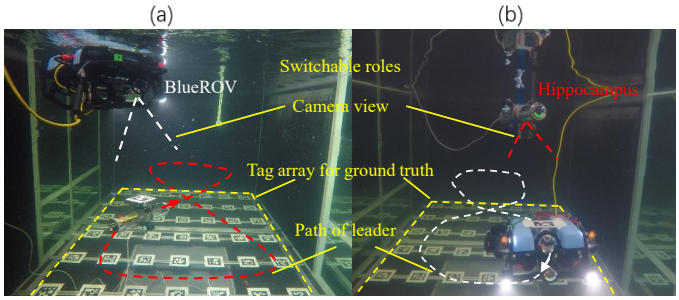

Fig. 7. Switchable leader-follower setup in an experimental tank. a) Underwater camera view when BlueROV2 follows HippoCampus (lead) which tracks an ∞-shaped path. b) HippoCampus switched to follower-mode with BlueROV2 (leader) doing self-navigation. Cables connected to both robots are for data recording. Tag arrays on the floor are for acquiring trajectory ground truth and to allow the leader's attitude navigation.

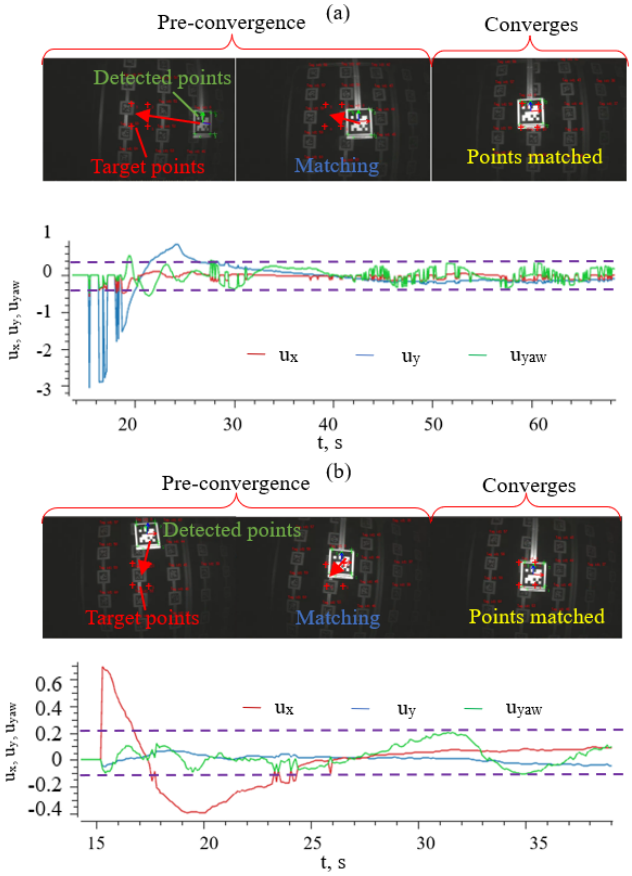

Fig. 8. Onboard camera view and velocity outputs during fixed tag tracking test. a) shows the maximum LoS in the robot's y-direction of the follower and feature points matching and velocity converging process, b) shows similar results but in x-direction.

floor are used to obtain ground truth for both trajectory tracking on the leader and data analysis. A unique AprilTag mounted on the top of the leader vehicle is used by the follower for tracking (see Fig. 7).

C. Experiments

Two sets of experiments were conducted with BlueROV2 acting as follower and one with HippoCampus trailing BlueROV2. To improve the visibility of the marker, flash-lights on the BlueROV were used. Using active, backlit markers as an alternative is the topic of ongoing research.

It should be noted that during our experiments, the follower robot's linear velocity gain in z direction from $\boldsymbol{K}_q$ was set to $k_z = 0$, whilst the depth of the leader is controlled by (8). Therefore, the proposed formation control in 3D environment was reduced to a 2.5D problem.

1) Tag tracking on a gantry fixed structure with BlueROV2: First, we focus our analysis on the performance of the visual servoing algorithm independent of the leader dynamics. For this, the target AprilTag was placed on the edge of the follower's camera field of view in the x and y- direction, respectively. This enables the convergence of the follower visual servoing towards the target feature to be studied. The results are shown in Fig. 8.

2) Multi-agent leader-follower formation: To achieve leader-follower formation control within the multi-agent system, we let the leader track an ∞-shape path at a constant depth, with the follower above the leader, as shown in Fig. 7. The goal is to have the follower repeat the motion the leader performs, i. e. the ∞-shape in this case. There is no active communication between the leader and follower, nor any human interaction during the tracking, and the role switch process was done manually. Furthermore, no localisation information was used for formation control (follower). The results are shown in Fig. 9 and Fig. 10.

D. Result and Discussion

1) Fixed tag tracking: As can be seen in Fig. 8, when the target tag appears on the edge of the robot's field of view, the follower-robot starts to adjust its displacement. The computed control effort for the corresponding direction initially peaks before the robot position quickly converges to the target. The computed control efforts decreased in a more unstable manner compared to results presented in [23] for simulation and [8] on a ground robot. In Fig. 8, camera distortion is noticeable around the edges. This was ignored in these experiments, but its effects will be investigated in future work.

The difference observed in our results compared to the in-air experiments is due to uncertainty in underwater robot dynamics such as drifts coupled with inaccuracies from underwater camera distortion. All of these are not fully compensated for adaptively by our current system. Our next stage

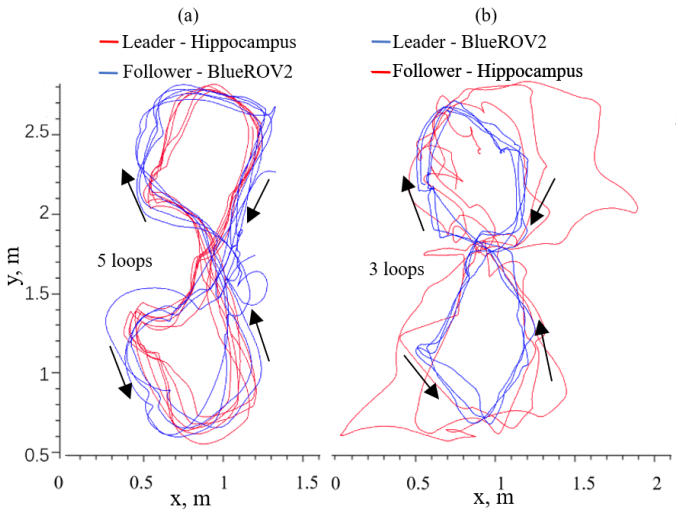

Fig. 9. Recorded paths of the leader and follower robots. a) Shows HippoCampus leading and BlueROV2 following, b) switched vice-versa BlueROV2 (leader) and HippoCampus (follower).

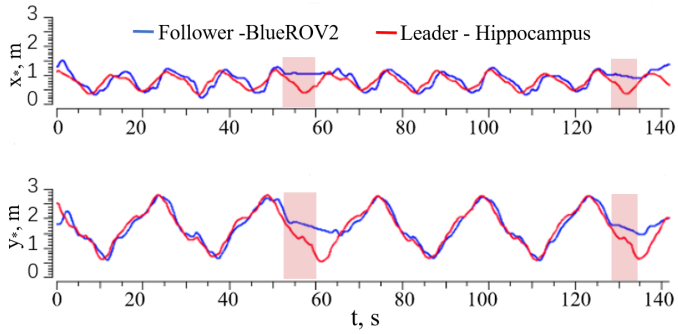

Fig. 10. Robot positions over time with BlueROV2 following HippoCampus. Pink areas indicate the time spans when the follower loses LoS to the leader.

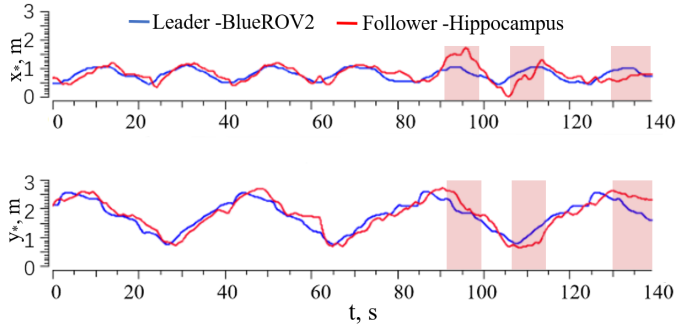

Fig. 11. Robot positions over time with HippoCampus following. Pink areas indicate the time spans when the follower loses LoS to the leader.

of development will set out to consider these limitations. Nevertheless, the control efforts converge within 30 seconds, similar to former literature. This demonstrates the feasibility of deploying such system on underwater platforms.

2) Leader-follower formation: Fig. 9 shows the xy positions of both, leader and follower, for the infinity shape trajectory. We observe that the follower successfully *copies* the behaviour of the leader. To be specific, for the BlueROV2 as follower, the maximum displacement in x-direction is 0.37 m and 0.41 cm for y-direction. The maximum projection distance in the xy plane is 0.45 m and occurs when the robot loses LoS during the tracking mission. Although LoS is lost at 53 seconds, the BlueROV2 follower catches the leader within 15 seconds without human interaction, see also Fig. 10. It is worth noticing that when loosing LoS, the x and y displacements between leader and follower are 0.18 m and 0.41 m, respectively. The x-displacement has not reached the maximum yet, which means the bottleneck of error tolerance lies in y-displacement. With HippoCampus as follower, the maximum displacement in x-direction, y-direction and projection distance in xy plane are 0.40 m, 0.50 m, and 0.42 m, as shown in Fig. 11. Results show the leader and follower are formatted with acceptable errors and instability.

V. CONCLUSION & FUTURE WORK

In this paper, we proposed a multi-agent heterogeneous system with a leader-follower formation control scheme in underwater scenarios. The control models were established with the IBVS algorithm deployed and tested on physical platforms. The results show the stability of feature points converging using IBVS and the feasibility of such a system operating underwater. Our demonstration is a clear example of working towards an underwater multi-agent system under constrained localisation and communication conditions. Our findings give a fundamental intuition on how well the IBVS approach works underwater for future researches, as they provide a reference of accessible methods for aquatic vision-based systems for developers in the community.

For the next stage of development, the AprilTag-based feature points will be replaced by more realistic source of feature point providers such as salient LED of optical modem or active markers. A motion prediction algorithm will be investigated for reducing the chance of losing LoS. Future development of formation control will also consider experiments in cluttered environments and the manual role switch process will be made autonomously. Moreover, dynamic model constraints of different robots will be considered to study the wider application on different platforms such as ASV/AUV systems.

REFERENCES

[1] S. Watson, D. A. Duecker, and K. Groves, "Localisation of unmanned underwater vehicles (uuvs) in complex and confined environments: A review," *Sensors*, vol. 20, no. 21, 2020. [Online]. Available: https://www.mdpi.com/1424-8220/20/21/6203

[2] S. Rahman, A. Q. Li, and I. Rekleitis, "Svin2: An underwater slam system using sonar, visual, inertial, and depth sensor," in *2019 IEEE/RSJ International Conference on Intelligent Robots and Systems (IROS)*, 2019, pp. 1861–1868.

[3] C. P. Bechlioulis, F. Giagkas, G. C. Karras, and K. J. Kyriakopoulos, "Robust formation control for multiple underwater vehicles," *Frontiers in Robotics and AI*, vol. 6, sep 2019.

[4] K. Groves, A. West, K. Gornicki, S. Watson, J. Carrasco, and B. Lennox, "Mallard: An autonomous aquatic surface vehicle for inspection and monitoring of wet nuclear storage facilities," *Robotics*, vol. 8, no. 2, 2019. [Online]. Available: https://www.mdpi.com/2218-6581/8/2/47

[5] D. A. Duecker, N. Bauschmann, T. Hansen, E. Kreuzer, and R. Seifried, "Towards micro robot hydrobatics: Vision-based guidance, navigation, and control for agile underwater vehicles in confined environments," in *2020 IEEE/RSJ International Conference on Intelligent Robots and Systems (IROS)*, 2020, pp. 1819–1826.

[6] E. Malis, F. Chaumette, and S. Boudet, "2 1/2 d visual servoing," *IEEE Transactions on Robotics and Automation*, vol. 15, no. 2, pp. 238–250, 1999.

[7] K.-K. Oh, M.-C. Park, and H.-S. Ahn, "A survey of multi-agent formation control," *Automatica*, vol. 53, pp. 424–440, 2015. [Online]. Available: https://www.sciencedirect.com/science/article/pii/S0005109814004038

[8] J. Lin, Z. Miao, H. Zhong, W. Peng, Y. Wang, and R. Fierro, "Adaptive image-based leader–follower formation control of mobile robots with visibility constraints," *IEEE Transactions on Industrial Electronics*, vol. 68, no. 7, pp. 6010–6019, 2021.

[9] A. Das, R. Fierro, V. Kumar, J. Ostrowski, J. Spletzer, and C. Taylor, "A vision-based formation control framework," *IEEE Transactions on Robotics and Automation*, vol. 18, no. 5, pp. 813–825, 2002.

[10] X. Liang, H. Wang, Y.-H. Liu, W. Chen, and T. Liu, "Formation control of nonholonomic mobile robots without position and velocity measurements," *IEEE Transactions on Robotics*, vol. 34, no. 2, pp. 434–446, 2018.

[11] F. Chaumette, "Image moments: a general and useful set of features for visual servoing," *IEEE Transactions on Robotics*, vol. 20, no. 4, pp. 713–723, 2004.

[12] L. Consolini, F. Morbidi, D. Prattichizzo, and M. Tosques, "Leader–follower formation control of nonholonomic mobile robots with input constraints," *Automatica*, vol. 44, no. 5, pp. 1343–1349, 2008. [Online]. Available: https://www.sciencedirect.com/science/article/pii/S0005109807004578

[13] X. Peng, Z. Sun, K. Guo, and Z. Geng, "Mobile formation coordination and tracking control for multiple nonholonomic vehicles," *IEEE/ASME Transactions on Mechatronics*, vol. 25, no. 3, pp. 1231–1242, 2020.

[14] X. Liang, H. Wang, Y.-H. Liu, Z. Liu, and W. Chen, "Leader-following formation control of nonholonomic mobile robots with velocity observers," *IEEE/ASME Transactions on Mechatronics*, vol. 25, no. 4, pp. 1747–1755, 2020.

[15] J. Wang, C. Wang, Y. Wei, and C. Zhang, "Filter-backstepping based neural adaptive formation control of leader-following multiple auvs in three dimensional space," *Ocean Engineering*, vol. 201, p. 107150, 2020. [Online]. Available: https://www.sciencedirect.com/science/article/pii/S0029801820302109

[16] H. Wang, D. Guo, X. Liang, W. Chen, G. Hu, and K. K. Leang, "Adaptive vision-based leader–follower formation control of mobile robots," *IEEE Transactions on Industrial Electronics*, vol. 64, no. 4, pp. 2893–2902, 2017.

[17] M. Dunbabin, P. Corke, I. Vasilescu, and D. Rus, "Experiments with cooperative control of underwater robots," *The International Journal of Robotics Research*, vol. 28, no. 6, pp. 815–833, 2009. [Online]. Available: https://doi.org/10.1177/0278364908098456

[18] E. Simetti, G. Indiveri, and A. M. Pascoal, "Wimust: A cooperative marine robotic system for autonomous geotechnical surveys," *Journal of Field Robotics*, vol. 38, no. 2, pp. 268–288, 2021. [Online]. Available: https://onlinelibrary.wiley.com/doi/abs/10.1002/rob.21986

[19] D. A. Duecker, N. Bauschmann, T. Hansen, E. Kreuzer, and R. Seifried, "Hippocampusx – a hydrobatic open-source micro auv for confined environments," in *2020 IEEE/OES Autonomous Underwater Vehicles Symposium (AUV)*, 2020, pp. 1–6.

[20] T. I. Fossen and O.-E. Fjellstad, "Nonlinear modelling of marine vehicles in 6 degrees of freedom," *Mathematical Modelling of Systems*, vol. 1, no. 1, pp. 17–27, 1995. [Online]. Available: https://doi.org/10.1080/13873959508837004

[21] D. A. Duecker, E. Kreuzer, G. Maerker, and E. Solowjow, "Parameter identification for micro underwater vehicles," in *Proceedings in Applied Mathematics and Mechanics (PAMM)*, vol. 18, no. 1, 2018, p. e201800350. [Online]. Available: https://onlinelibrary.wiley.com/doi/abs/10.1002/pamm.201800350

[22] J. Chen, C. Sun, and A. Zhang, "Autonomous navigation for adaptive unmanned underwater vehicles using fiducial markers," in *2021 IEEE International Conference on Robotics and Automation (ICRA)*, 2021, pp. 9298–9304.

[23] F. Chaumette and S. Hutchinson, "Visual servo control. i. basic approaches," *IEEE Robotics & Automation Magazine*, vol. 13, no. 4, pp. 82–90, 2006.

[24] Z. Zhou, Y. Jiang, Y. Li, C. Jian, and Y. Sun, "A single acoustic beacon-based positioning method for underwater mobile recovery of an auv," *International Journal of Advanced Robotic Systems*, vol. 15, no. 5, p. 1729881418801739, 2018. [Online]. Available: https://doi.org/10.1177/1729881418801739

[25] D. A. Duecker, A. Hackbarth, T. Johannink, E. Kreuzer, and E. Solowjow, "Micro underwater vehicle hydrobatics: A submerged furuta pendulum," in *2018 IEEE International Conference on Robotics and Automation (ICRA)*, 2018, pp. 7498–7503.

[26] E. Marchand, F. Spindler, and F. Chaumette, "Visp for visual servoing: a generic software platform with a wide class of robot control skills," *IEEE Robotics & Automation Magazine*, vol. 12, no. 4, pp. 40–52, 2005.